Reproducing Evacuation Behaviors of Evacuees during the Great East Japan Earthquake using the Evacuation Decision Model with Realistic Settings

Akira Tsurushima[a]
Intelligent Systems Laboratory, SECOM CO., LTD., Mitaka, Tokyo, Japan

Keywords: Evacuation Decision Model, Herd Behavior, Functional Field of View, Tunnel Vision.

Abstract: The analysis of evacuation behaviors from the video captured during the Great East Japan Earthquake revealed that the evacuation behaviors of fleeing and dropping down were affected by the distance from the exits. These behaviors were reproduced through simulations by employing the evacuation decision model, which is a model of herd behaviors during evacuations; this showed that these unique evacuation behaviors could be reproduced by simple herd behaviors. However, the results are questionable owing to the oversimplified settings of the simulations, such as the different number and density of agents and the overlooked physical constraints. We conduct simulations with settings that are more representative of those in the video clip. The unique evacuation behavior is also reproduced with our simulation setting but for limited ranges of parameter values. The analysis of the results reveals that the parameters related to the vicinity of an agent are significant; this lead to the hypothesis that the attention of evacuees is narrowed to 20 degrees with a relatively long range during evacuations.

1 INTRODUCTION

The fields of pedestrian dynamics, collective behaviors, and crowd evacuations have gathered massive attention from researchers; owing to this, several studies have been conducted on these fields, and the associated literature has rapidly increased (Haghani, 2020a; Haghani, 2020b). Although several researchers consider the effects of cognitive or psychological factors in disaster evacuations to be significant (Sieben et al., 2017; Haghani et al., 2016), little is known about the mental mechanisms and cognitive processes of these factors owing to the difficulties involved in obtaining objective data. Therefore, studies on human evacuation behaviors are usually conducted through interviews of survivors (Mas et al., 2012; Drury et al., 2015), laboratory experiments with humans (Schmidt and Galea, 2013; Garcimartín et al., 2014; Haghani et al., 2016) or animal subjects (Saloma et al., 2003; Ji et al., 2017), and literature studies. However, these methods have limitations in terms of objectivity; for example, reproducing mental stress of real evacuations in laboratory experiments is difficult, and methods employing interviews or surveys are subject to survivorship bias. With the increase in surveillance cameras and smartphones, videos and images of disaster evacuations have been accrued; novel approaches to investigate evacuation behaviors have emerged by analyzing these videos (Yang et al., 2011; D'Orazio et al., 2014; Gu et al., 2016).

Tsurushima (2020) combined multi-agent simulations with video analysis to investigate human evacuation behaviors during an earthquake. This study analyzed a video clip captured during the Great East Japan Earthquake and discovered unique human evacuation behavior that showed that distances to exits determine the choice of actions between fleeing the room and dropping under the table (Tsurushima, 2020). This unique evacuation behavior was reproduced by multi-agent simulations using the evacuation decision model (Tsurushima, 2019), a model of human herd behavior, which shows a cognitive bias during evacuations (Altshuler et al., 2005; Helbing et al., 2000; Lovreglio et al., 2014; Raafat et al., 2009). Tsurushima concluded that simple herd behaviors are sufficient to reproduce the unique evacuation behavior.

The research revealed the effects of herd behavior on evacuations and reproduced diagonal spatial patterns of the choices between fleeing and dropping

[a] https://orcid.org/0000-0003-2711-297X

Tsurushima, A.
Reproducing Evacuation Behaviors of Evacuees during the Great East Japan Earthquake using the Evacuation Decision Model with Realistic Settings.
DOI: 10.5220/0010167700170027
In *Proceedings of the 13th International Conference on Agents and Artificial Intelligence (ICAART 2021) - Volume 1*, pages 17-27
ISBN: 978-989-758-484-8

through simulations; however, the results are questionable owing to the oversimplified configurations of these simulations. In the video, 48 people were arranged in a square facing the center of the room; their movements were constrained by desks and chairs. In contrast, in the simulation settings, 500 people were evenly distributed across the room; their movements were unconstrained. These differences are not negligible because, in the evacuation decision model, herd behaviors are determined by the movements of others in the vicinity of each agent. Thus, these differences may result in different results.

In this study, we reexamine the works of (Tsurushima, 2020) through simulations using the same model but with more realistic simulation settings; we investigate whether the results hold under the new settings. We also analyze the conditions in which and the reasons why the evacuation decision model reproduces the unique evacuation behaviors captured in the video clip. The results of the analysis yield a hypothesis based on human cognitive factors, which affect evacuation behaviors, that might be difficult to be obtained by empirical studies.

2 EVACUATION BEHAVIOR DURING THE GREAT EAST JAPAN EARTHQUAKE

In this section, we briefly describe the work of (Tsurushima, 2020) including the unique evacuation behavior reported, the evacuation decision model, and the configurations and results of the simulations. We also mention the differences in the simulation configurations compared to the real situations in the video clip.

2.1 Diagonal Spatial Pattern

From the analysis of the video clip [1] captured during the Great East Japan Earthquake, Tsurushima (2020) reported unique evacuation behaviors of people, in which choosing between fleeing the room and dropping under tables was decided based on the distances to the exits. Figure 1 shows the initial positions of 48 people at the start of the earthquake in a square room with only one exit at the lower right corner. Figure 2 shows the result of the video analysis, in which a diagonal spatial pattern of the evacuees' choices between fleeing and dropping emerged at the end of the earthquake depending on their distances to the exit. A white triangle denotes an evacuee who chose to flee and a black triangle denotes an evacuee who chose to drop. A gray triangle denotes an evacuee whose choice is unknown.

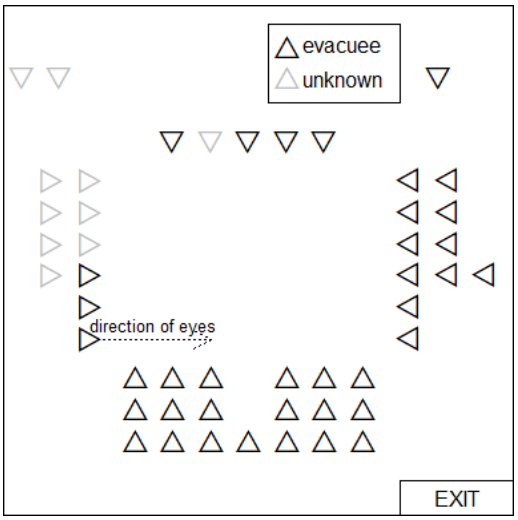

Figure 1: Initial positions of 48 people in the room. Each faces the center of the room.

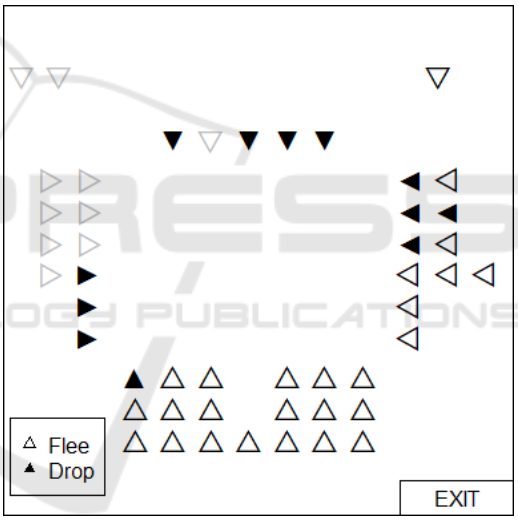

Figure 2: Final choices of either fleeing or dropping.

A simple theory to describe the phenomenon is that an evacuee determines the choice between fleeing and dropping based on his/her distance to the exit. Instead of the simple theory, Tsurushima made a hypothesis that evacuees make a random choice between fleeing and dropping; however, herd behaviors among evacuees result in a diagonal spatial pattern.

2.2 Evacuation Decision Model

The diagonal spatial pattern of fleeing and dropping evacuees was reproduced by simulations using the

[1] https://www.youtube.com/watch?v=tejlDDKeg8s

evacuation decision model, which is a model of herd behavior during human evacuations.

In the evacuation decision model, agent a_i has a variable $X_i \in \{0,1\}$; a_i decides his/her behavior either by himself/herself if $X = 1$ or by herd behavior if $X = 0$. The values of X toggles between 0 and 1 with the following transition probabilities:

$$P(X_i = 0 \to X_i = 1) = \frac{s_i^2}{s_i^2 + \theta_i^2}, \quad (1)$$

$$P(X_i = 1 \to X_i = 0) = \varepsilon, \quad (2)$$

where s_i is a local estimate of the stimulus from the environment for a_i, θ_i is the response threshold of a_i, and ε is a constant probability common for all agents. A local estimate of the stimulus from the environment is calculated as follows:

$$s_i(t+1) = max\{s_i(t) + \delta - \alpha(1-R)F,\ 0\}, \quad (3)$$

where δ is the increase of the stimulus per unit time and α is the scale factor of the stimulus. R, the risk perception function of objective risk r, is defined as follows:

$$R(r) = \frac{1}{1 + e^{-g(r-\mu_i)}}, \quad (4)$$

where g is the activation gain of the sigmoid function and μ_i is the risk perception factor of a_i, which represents the individual sensitivity to risk. r represents the objective risk in the environment, which is given as follows:

$$r(t+1) = r(t) + \Delta r \quad (5)$$

and $r(0) = 0$. F is the evacuation progress function of a_i that estimates the total progress of the evacuation:

$$F(n) = \begin{cases} 1 - n/\hat{N} & n < \hat{N} \\ 0 & \text{otherwise,} \end{cases} \quad (6)$$

where n is the number of agents in the vicinity and $\hat{N}$ is the maximum possible number of agents in the vicinity. The vicinity of an agent is defined by distance d (units) and angle ω (degrees) from the direction in which the agent is headed. Depending on the value of X_i, a_i performs one of the following actions:

1. if $X_i = 1$, randomly chooses to either flee or drop, or
2. if $X_i = 0$, chooses to flee or drop, or his/her action is undetermined depending on the most popular action in the vicinity.

No agent estimates the distance to the exit or chooses his/her behavior based on the distance.

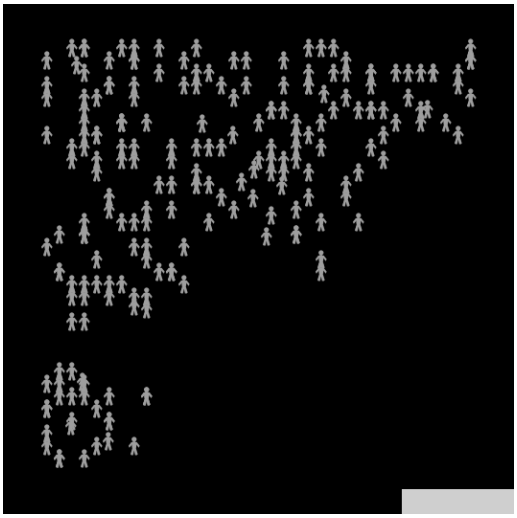

Figure 3: Example of the diagonal spatial pattern. All fleeing agents went out through the exit and all dropping agents were in the room. A diagonal border between fleeing and dropping agents has emerged.

2.3 Simulation A

Hereinafter, we refer to the simulations in (Tsurushima, 2020) as simulation A. In simulation A, 500 agents incorporating the evacuation decision model were evenly distributed in a square space (40×40 units) with only one exit at the lower right corner (Fig. 3). The parameters used in simulation A were as follows: $\alpha = 1.2$, $\delta = 0.5$, $\varepsilon = 0.2$, $g = 1.0$, $\hat{N} = 10$, $d = 5$, and $\omega = 120$.

Figure 3 illustrates an example of the simulation results showing a diagonal spatial pattern of fleeing and dropping evacuees; the unique evacuation behavior captured in the video (a diagonal spatial pattern) is reproduced by the evacuation decision model.

2.4 Critical Analysis

Tsurushima (2020) concluded that simple herd behavior is sufficient to reproduce the diagonal spatial pattern because all actions by agents in simulation A are either random or herd behavior. However, the initial condition of simulation A might not be considered as the same as that of the real situation captured in the video; therefore, the results of the study are questionable.

The environment of simulation A, which is a square room with one exit at one corner, can be a good representation of the real situation in the video. However, the number of agents and their initial layout in the room are very different from the real situation. The number of agents in simulation A was 500,

whereas there were 48 agents in the real situation. The agents were evenly distributed across the room with high density in simulation A, whereas people were arranged in a square with relatively sparse density in the real situation. Furthermore, agents faced random directions in simulation A, whereas all the people in the video faced the center of the room.

In the video, tables and chairs were laid out in a square shape in the room and the movements of people were physically restricted by these objects. However, the movements of the agents in simulation A were unrestricted; agents could move directly toward the exit. In the evacuation decision model, the decision of an agent is determined by the behaviors of other agents in the vicinity of that agent. Thus, the position of an agent in the room will affect the decisions of other agents and vice versa. The following factors can significantly affect the overall dynamics of the behavior of the model.

1. Constraints against the movement of an agent.
2. Vicinity of an agent (direction in which the agent is facing).
3. Distribution of agents in the room.

Therefore, the differences between the configurations of simulation A and those of the real situation are not negligible. A more extensive analysis of these differences is required.

3 EXPERIMENT

In this section, we describe simulations using the evacuation decision model with more realistic configurations (we will call them simulation B) and examine whether the diagonal spatial pattern reported by Tsurushima (2020) can be reproduced with these settings.

3.1 Simulation B

Figure 4 depicts the initial positions of 48 agents in a square space (15×15 units), which has one exit at the lower right corner. All the agents face toward the center of the room, as in the video clip.

Figure 5 illustrates the constraints on the movements of these agents. A circle on a grid refers to the initial position of an agent. An arrow on a grid shows the direction of movement that agents on those grids must follow. For example, the red agent in the upper left in the figure can only move to the right. Grey grids show the area where the movements of agents are unrestricted. Thus, when an agent reaches one of these grids, he/she can move directly to the exit.

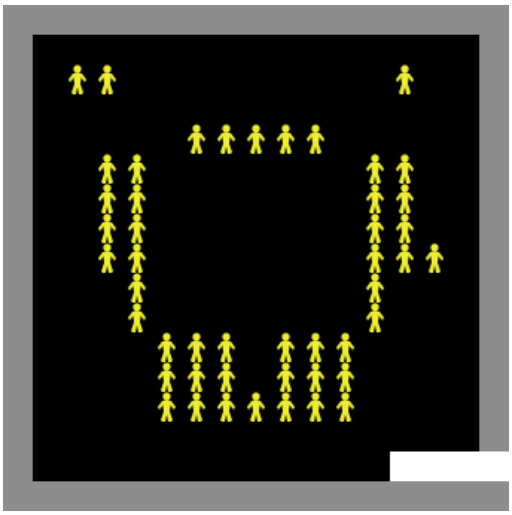

Figure 4: Initial positions of 48 agents.

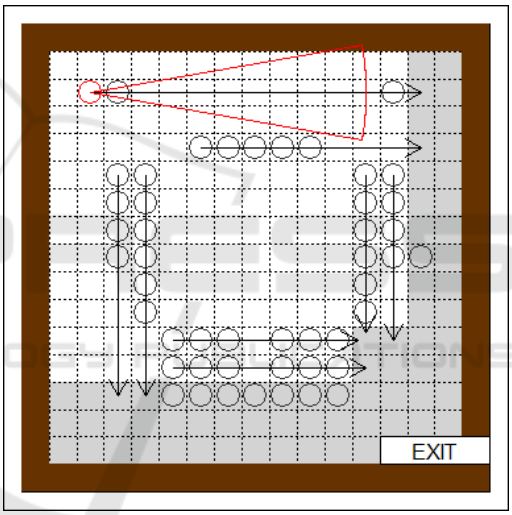

Figure 5: Constraints on the movement of agents. Arrows depict the movement direction. Grey area shows the area where the movements of agents are unrestricted. The red fan shape shows the field of view of the red agent on the upper left corner.

In simulation A, an agent is unrestricted physically, and therefore can pass through other agents standing on the way to the exit. In contrast, the agents in simulation B are constrained physically; hence, agents in this setting are unable to pass through other agents. They must stop whenever other agents are in front of them.

Although the configurations are different, an agent incorporating the evacuation decision model is identical to the one employed in simulation A. The parameters used in simulation B are as follows: $\alpha = 0.4$, $\delta = 1.0$, $\varepsilon = 0.1$, $g = 0.7$, $\hat{N} = 10$, $d = 10$, $\omega = 20$, and $\Delta r = 2.0$.

Algorithm 1: Herd Behavior ($X = 0$).

$n_d \Leftarrow |\{a_j \in V_i | \pi_j(t) = drop\}|$
$n_e \Leftarrow |\{a_j \in V_i | \pi_j(t) = flee\}|$
$n_u \Leftarrow |\{a_j \in V_i | \pi_j(t) = undecided\}|$
if $n_d > n_e$ and $n_d > n_u$ **then**
  $\pi_i(t) \Leftarrow drop$
else if $n_e > n_d$ and $n_e > n_u$ **then**
  $\pi_i(t) \Leftarrow flee$
end if
if $\pi_i(t) = flee$ **then**
  move 1 unit following the constraints in Fig. 5.
end if

Algorithm 2: Random Selection ($X = 1$).

if $\pi_i(t) = undecided$ **then**
  $\tau \sim U(0,1)$
  if $\tau \leq 0.5$ **then**
    $\pi_i(t) \Leftarrow drop$
  else
    $\pi_i(t) \Leftarrow flee$
  end if
end if
if $\pi_i(t) = flee$ **then**
  move 1 unit following the constraints in Fig. 5.
end if

3.2 Simulation Model

In this section, we briefly describe the simulation algorithms employed in the experiments. The algorithms are identical to those used by Tsurushima (2020).

$A = \{a_1, a_2, \ldots, a_{48}\}$ is a set of 48 agents assigned in the square space, as shown in Fig. 4. An agent a_i has a variable $\pi_i(t) = \{drop, flee, undecided\}$ holding a current decision. The vicinity of a_i is defined as $V_i = \{a_j \in A | \upsilon(a_j, a_i)\}$, where $\upsilon : A^2 \rightarrow \{true, false\}$, and υ refers to a fan-like range of d units ω degrees toward the direction of motion of a_i.

Algorithm 1 describes the action of a_i with $X_i = 0$ (herd behavior), and Algorithm 2 describes the action of a_i with $X_i = 1$ (random selection). Assuming a simulation time $t = 1, \ldots, T$, the overall procedure is given in Algorithm 3.

NetLogo 6.1.1 (Wilensky, 1999) was used to implement the algorithms described in this section.

3.3 Result

Figure 6 depicts an example result of simulation B. Similar to the result of simulation A (Fig. 3), the agents that remained were on the far left from the exit in the space, resulting in a diagonal spatial pattern.

Algorithm 3: Simulation.

for $t = 1$ to T **do**
  $r \Leftarrow min\{r + \Delta r, 100\}$
  for all $a_i \in A$ **do**
    Caluculate s_i, R, and F (eq. 3, 4, and 6)
    $\tau \sim U(0,1)$
    if $X_i = 1 \wedge \tau < P(X_i = 1 \rightarrow X_i = 0)$ **then**
      $X_i \Leftarrow 0$
      Execute Algorithm 1 {Herd Behavior}
    else if $X_i = 0 \wedge \tau < P(X_i = 0 \rightarrow X_i = 1)$ **then**
      $X_i \Leftarrow 1$
      Execute Algorithm 2 {Random Selection}
    end if
    if a_i is on the exit **then**
      $A \Leftarrow A \setminus a_i$
    end if
  end for
end for

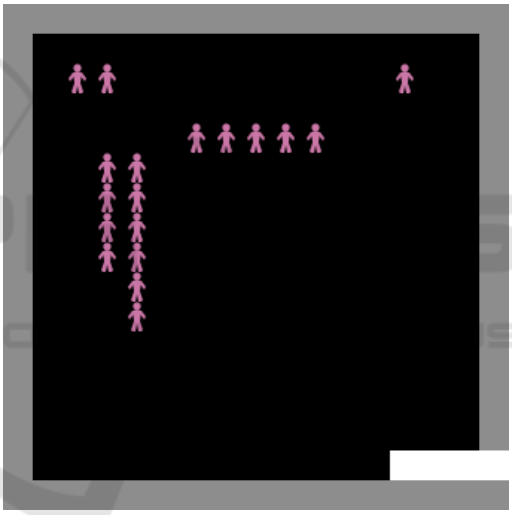

Figure 6: Example result of simulation B.

The results similar to Fig. 3 are not necessarily obtained because of the stochastic nature of the model. Thus, we conducted 300 simulations to confirm the generality of the results.

Figure 7 shows the heat map of the results of 300 simulations. The dark area indicates a high frequency of remaining agents and the light area indicates a low frequency of remaining agents. Similar to simulation A, agents that remained were far from the exit; none or very few agents remained in areas close to the exit. Note that we employed the logarithm of the frequency of the number of remaining agents when creating the heat map because the frequency varies significantly.

Now, we can conclude that the behaviors captured in the video clip in (Tsurushima, 2020) can be reproduced by simulation B as well as simulation A.

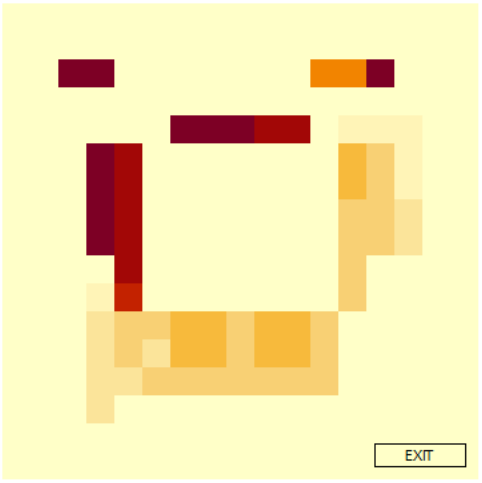

Figure 7: Heat map of the results of 300 simulations.

4 ANALYSIS

Practically, obtaining the result presented in section 3.3 was quite challenging owing to the parameter sensitivity of the model. Most sets of parameters failed to produce the diagonal spatial pattern captured in the video. Thus, we employed black-box optimization techniques to explore parameter sets that can reproduce the diagonal spatial pattern, which discriminates between fleeing and dropping behaviors as shown in the video.

For this, an objective function that evaluates the simulation results in terms of the diagonal spatial pattern is required. By considering the center of the room as the origin, the objective function must take the following two conditions into account.

1. Maximize the number of agents above $y = x$; minimize those below $y = x$.
2. Make the number of agents symmetrical with respect to $y = -x$; i.e., minimize the absolute value of the difference between the numbers of agents above and below $y = -x$.

Let the coordinates of agent a_i be (x_i, y_i). Condition 1 can be expressed by maximizing:

$$L^+ = \sum_{\{a_i | y_i \geq x_i\}} l_i^+ - \sum_{\{a_j | y_j < x_j\}} l_j^+, \tag{7}$$

where l_i^+ is the distance between a_i and $y = x$.

$$l_i^+ = \sqrt{2\left(\frac{x_i - y_i}{2}\right)^2}. \tag{8}$$

Condition 2 can be expressed by minimizing:

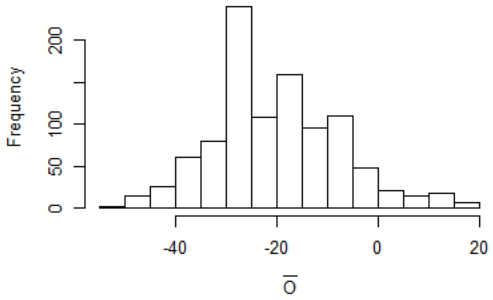

Figure 8: Histogram of the values of $\bar{O}$ for 1000 simulations with random parameters.

$$L^- = \left| \sum_{\{a_i | y_i \geq -x_i\}} l_i^- - \sum_{\{a_j | y_j < -x_j\}} l_j^- \right|, \tag{9}$$

where l_i^- is the distance between a_i and $y = -x$.

$$l_i^- = \sqrt{\left(x_i + \frac{y_i - x_i}{2}\right)^2 + \left(y_i - \frac{y_i - x_i}{2}\right)^2}. \tag{10}$$

Thus, the black-box optimization problem mentioned above is to maximize

$$max \quad O = L^+ - L^- \tag{11}$$

with respect to the domains of the parameters in the evacuation decision model.
In the case of the result shown in section 3.3, the value of O was 42.43.

Figure 8 shows the histogram of the values of $\bar{O}$ for 1000 simulations for random parameters of the evacuation decision model. $\bar{O}$ is the mean of the value of Os for 100 simulations with a given set of parameters. The range of $\bar{O}$ is $-54.06 \leq \bar{O} \leq 17.37$. Figure 8 illustrates that $\bar{O}$ is negative in most cases; only 6% have a positive $\bar{O}$. The result described in section 3.3, which necessarily has a positive O, is not easily obtained by the evacuation decision model; a careful choice of parameter values is required to reproduce the diagonal spatial pattern.

4.1 Black-box Optimization

We conducted black-box optimization to search for parameters that can reproduce the diagonal spatial pattern. We employed simulated annealing as a search algorithm and the mean of 100 simulation samples ($\bar{O}$) as the objective function in the search. Therefore, the objective function was evaluated every 100 simulations. We conducted the search 20 times with different initial points and 1000 iterations each.

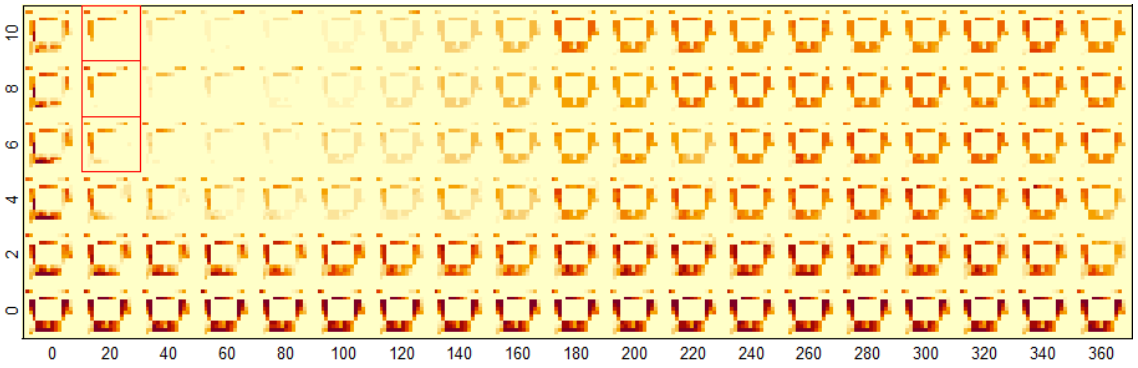

Figure 9: Results of sensitivity analysis for d and ω. The rows show d and the columns show ω. Each cell shows the heat map of 100 simulations. Cells with red square frames refer to the result for $\bar{O} > 10$.

Table 1: Top 5 results of black-box optimization.

ε	δ	α	d	ω	Δr	$\hat{N}$	g	$\bar{O}$
0.1	1.2	0.1	10	20	5.0	15	0.4	28.95
0.1	0.7	0.4	10	20	2.0	1	1.5	27.76
0.1	1.1	0.8	8	20	5.0	2	1.4	26.64
0.2	0.6	0.6	9	20	2.5	7	1.4	26.23
0.1	1.0	0.2	10	20	1.5	20	0.2	26.22

Table 1 shows the top five results of the black-box optimization; the complete table is given in the Appendix. The maximum value of the objective function found in 20 trials of black-box optimization was $\bar{O} = 28.95$. Table 1 shows that the top five results have some common parameter values, such as $\varepsilon \leq 0.2$, $d \geq 8$, and $\omega = 20$.

4.2 Multiple Regression Analysis

We investigated the statistical significance of each parameter against the objective value ($\bar{O}$) using multiple regression analysis. To conduct multiple regression analysis, we randomly chose 100 samples from 1000 samples, from the results of simulations with random parameters, as shown in Fig. 8. The result of the analysis ($P < 0.001$) is given in Table 2. The top row shows the coefficients of the parameters and the bottom row shows the corresponding P-values.

Table 2: Result of multiple regression analysis.

	ε	δ	α	d	ω	Δr
Coef	7.68	3.21	1.42	1.50	-0.06	1.18
P-val	0.01	0.06	0.36	0.00	0.00	0.05
	$\hat{N}$	g				
Coef	0.12	-1.81				
P-val	0.50	0.35				

The result reveals that d and ω are statistically significant ($P < 0.001$), implying that the vicinity of an agent affects the simulation results significantly. Furthermore, ε is also statistically significant ($P < 0.01$). Note that we randomly chose 100 samples from 1000 from Fig. 8 to avoid the decrease in P-value owing to the large size of the data.

4.3 Sensitivity Analysis

We conducted a sensitivity analysis for parameters d and ω to examine the effects of these parameters on the simulation results by varying d from 0 to 10 and ω from 0 to 360. We conducted 100 simulations for each combination of d and ω. The coordinates of all agents that remained at the end of the simulation were recorded; these coordinates were represented as a heat map of the result of the analysis.

Figure 9 shows the heat maps of the results of the simulations for each combination of parameters. The rows in the figure show the values of d and the columns show the values of ω. Each cell depicts the positions of the remaining agents at the end of the simulations. Dark colors show the high-frequency positions and light colors show low-frequency positions. Figure 9 illustrates that most combinations of parameters lead to spatial patterns that are dissimilar to the one in the video clip. Only a few cells at the upper left in the figure show a diagonal spatial pattern. The red square frames in the figure refer to the combinations of d and ω with $\bar{O} > 10$. This reveals that only parameters with $d \geq 8$ and $\omega = 20$ will lead to the occurrence of diagonal spatial patterns. This result is in good agreement with the result in section 4.1.

Furthermore, we conducted a sensitivity analysis for ε, another significant parameter discussed in section 4.2, which is the transition probability of $X = 1$ to $X = 0$. We conducted 100 simulations with ε varying from 0.1 to 1.0. The values of d and ω were fixed to 10 and 20, respectively, during the analysis. The

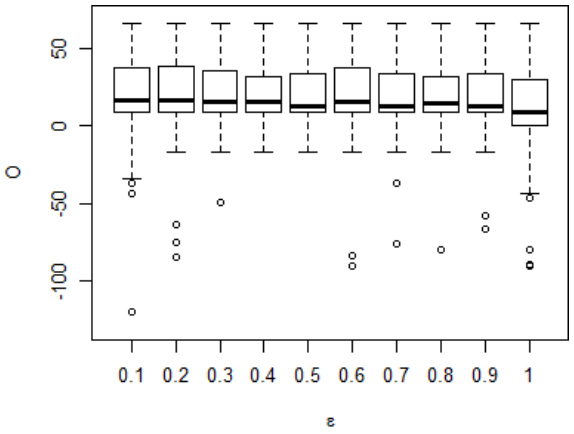

Figure 10: Results of sensitivity analysis for ε. Y-axis depicts the values of O.

results are presented as a box-and-whisker diagram in Fig. 10. The x-axis represents ε and the y-axis represents O. The figure illustrates that the value of ε does not affect simulation results much as long as the values of d and ω are within a certain range, implying that the transition probability of intentional behaviors ($X = 1$) to herd behaviors ($X = 0$) is unrelated to the occurrence of a diagonal spatial pattern.

5 DISCUSSION

Section 3.3 showed that simulations with more realistic settings (simulation B) can reproduce the diagonal spatial pattern, similar to simulation A, of an evacuee's choice between fleeing and dropping observed in the video clip captured during the Great East Japan Earthquake. However, this is only true for limited ranges of parameters.

Analysis in section 4.2 revealed that d and ω are statistically significant; the occurrence of a diagonal spatial pattern is affected by these two parameters. Black-box optimization in section 4.1 explored the values of these parameters that will result in a diagonal spatial pattern, which were $d \geq 8$ and $\omega = 20$. The sensitivity analysis in section 4.3 illustrated that diagonal spatial patterns are scarcely observed outside the specified ranges of these two parameters. A diagonal spatial pattern was not obtained using the parameter settings employed in simulation A, i.e., $d = 5$ and $\omega = 120$.

Both d and ω are related to the definition of the vicinity of an agent. The vicinity of an agent is assumed to have a fan-like shape with a length of d and angle of ω degrees in the direction in which the agent is headed. The red fan shape in Fig 5 illustrates the vicinity ($d = 10$ and $\omega = 20$) of the red agent on the upper left in the figure. This definition of vicinity can be considered to be narrow and lengthy because the size of the space is only 15×15 units. In the evacuation decision model, the herd behavior of an agent is affected by other agents within his/her vicinity; therefore, the vicinity of an agent can be considered as the field of vision or the range of attention of the agent. The analysis in section 4 leads to the following hypothesis.

Tunnel Vision Hypothesis. *During evacuations, the attention of evacuees is narrowed to a range of 20 degrees with a relatively long distance.*

This fact, i.e., the attention of evacuees focused on a very narrow and lengthy range in the direction of travel during an event of a major disaster such as the Great East Japan Earthquake, may have important implications for understanding human evacuation behaviors. The evacuation decision model is a constructive model and only generates sufficient conditions; different model assumptions may lead to different results. For example, the assumption that an agent selects between fleeing and dropping based on the distance from the exit individually will lead to the functional field of view of an evacuee being independent of the evacuation decisions; our study does not rule out the possibility of such a theory. Because, in our study, random selection does not produce any bias in the spatial pattern of agents, herd behaviors embedded in the evacuation decision model can be considered a crucial assumption in deriving the tunnel vision hypothesis. Although the tunnel vision hypothesis is merely a sufficient condition, the generation of such a hypothesis has some significance because collecting data in real evacuation situations is difficult, much less the exploration of internal models of evacuees' perceptions.

6 RELATED WORKS AND GENERAL DISCUSSION

Mackworth introduced the concept of the functional field of view (FFOV) as *the area around the fixation point from which information is briefly stored and read out during a visual task* (Mackworth, 1965). The FFOV narrows to prevent mental overload in the case of excessive cognitive demands in visual tasks; Mackworth called this phenomenon *tunnel vision*. Stressful, emotional, or unsafe events cause a narrower FFOV and inhibit the memory of peripherals, which is also known as *weapon focus effect*. Loftus et al. (1987) showed that memory related to a weapon and details of the hand holding it is im-

proved at the expense of the memory of the face and objects in peripheral vision (Loftus et al., 1987). Similar results, i.e., emotional arousal improves memory for central information but undermines memory of peripheral information, were reported by several researchers; however, the concept of central information was somewhat ambiguous (Christianson and Loftus, 1987; Christianson, 1992). Burke et al. (1992) discriminated central information into episode centrality and spatial centrality and revealed that emotional arousal prevents only the memory of spatially peripheral information (Burke et al., 1992). Harada et al. (2020) also reported that both unusualness and unsafety play a role in impairing the FFOV (Harada et al., 2020).

The narrowing of the FFOV in everyday lives was studied within the context of driving. Miura (1986) measured the FFOV of drivers during driving and found that the FFOV narrowed as traffic congestion increased (Miura, 1986). Recarte and Nunes (2003) investigated the effects of mental workload tasks on visual-detection and discrimination tests during driving (Recarte and Nunes, 2003). Mental tasks resulted spatial gaze concentration and visual-detection impairment by assigning attentional resources to the mental tasks rather than employing tunnel vision.

These studies reveal that stressful, unusual, and unsafe situations lead to tunnel vision, i.e., narrowing of the FFOV; this implies that tunnel vision may occur under evacuation situations because evacuations lead to all of these factors. However, studies have not focused much on tunnel vision under evacuation conditions. The study of human vision during evacuations has mainly been investigated under two contexts: identification of evacuation signs (Nilsson et al., 2009; Galea et al., 2014; Li et al., 2017; Ding et al., 2020; Bae et al., 2020) and evacuation behaviors under limited visibility conditions (Latané and Darley, 1968; Nilsson and Johansson, 2009; Li et al., 2019). Several researchers conducted experiments using eye-tracking devices to investigate the direction in which evacuees were looking during evacuations (Li et al., 2017; Ding et al., 2020; Bae et al., 2020). Although these works do not focus on the FFOV of evacuees, the devices may be useful to reveal the FFOV and tunnel vision effects during evacuations.

Numerous evacuation simulations consider the field of view of evacuees in their models; yet, effects of tunnel vision of evacuees during evacuations have barely been considered seriously. These simulations employ the cellular automaton-based model (Yue et al., 2010; Xu and Huang, 2012; Li et al., 2019) and the social force model (Ma et al., 2017; Yuan et al., 2017; Zhou et al., 2018). All of these assume the visibility of an agent based on distance; this implies that the visual field of the agent is a simple circle. Filippidis et al. (2006) introduced the concept of visibility catchment area (VCA), which is the physical visibility range of an evacuation sign (Filippidis et al., 2006). They also assumed that an agent could recognize the evacuation sign in the VCA based on the probability obtained by the relative angle between the location of the sign and the traveling vector of the agent. These probabilities were arbitrarily selected and unchanged during simulations.

Empirical studies on human evacuation behaviors through interviews, surveys, or laboratory experiments have limitations owing to the difficulty in obtaining objective data because the mental stress and distress under real evacuations are difficult to be reproduced. Constructive studies like simulations and modeling might be beneficial if employed in conjunction with empirical results; however, the results of constructive approaches only lead to sufficient conditions. The hypothesis we generated in this study, which is that the range of attention of evacuees narrows to an angle of 20 degrees in the traveling vector direction, may have been difficult to be obtained through empirical approaches.

Studies on tunnel vision and weapon focus effect reveal that the FFOV narrows under stressful or unusual situations. These results are likely to support our hypothesis because evacuation situations are considered to be stressful, unusual, and unsafe. Studies on evacuation behaviors with narrowed visual fields have not been conducted extensively; thus, the effect of these behaviors in evacuation situations is unknown. It will be beneficial to unveil human evacuation behaviors with a narrowed FFOV because this may alter evacuation plans and designs, which may lead to reduction in the number of casualties. Our hypothesis regarding which circumstances of evacuations will narrow the FFOV of evacuees is yet to be validated. Empirical studies to validate our hypothesis will also be valuable and desirable.

7 CONCLUSION

Through simulations using the evacuation decision model, unique evacuation behaviors of the distance from exits affecting the choice between fleeing and dropping actions have been reproduced. We conducted simulations with the same model but with more realistic configurations and revealed that unique evacuation behaviors could be reproduced in our settings for limited parameter ranges. The analysis showed that two parameters related to the vicinity of

an agent are significant; the unique behaviors could be reproduced only for certain values of these parameters. Our research leads to the hypothesis that the FFOV of evacuees is narrowed to an angle of 20° with a relatively long distance. As this hypothesis may alter the development and design of previously accepted evacuation protocols, the validation and application of the hypothesis to the real environment would be desirable; however, these are left for future works.

ACKNOWLEDGEMENTS

The author is grateful to Kei Marukawa for his helpful comments and suggestions. The author would like to thank Editage (www.editage.com) for English language editing.

REFERENCES

Altshuler, E., Ramos, O., Nuñez, Y., Fernańdez, J., Batista-Leyva, A. J., and Noda, C. (2005). Symmetry breaking in escaping ants. *The American Naturalist*, 166(6):643–649.

Bae, Y.-H., Kim, Y.-C., Oh, R.-S., Son, J.-Y., Hong, W.-H., and Choi, J.-H. (2020). Gaze point in the evacuation drills: Analysis of eye movement at the indoor wayfinding. *Sustainability*, 12(2902):1–14.

Burke, A., Heuer, F., and Reisberg, D. (1992). Remembering emotional events. *Memory and Cognition*, 20:277–290.

Christianson, S.-A. (1992). Emotional stress and eyewitness memory: A critical review. *Psychological Bulletin*, 112(3):284–309.

Christianson, S.-A. and Loftus, E. F. (1987). Memory for traumatic events. *Applied Cognitive Psychology*, 1:225–239.

Ding, N., Chen, T., and Liu, Y. (2020). Evacuation guidance design: An experimental study based on eye tracking devices. *Collective Dynamics*, 5.

D'Orazio, M., Spalazzi, L., Quagliarini, E., and Bernardini, G. (2014). Agent-based model for earthquake pedestrians' evacuation in urban outdoor scenarios: Behavioural patterns definition and evacuation paths choice. *Safety Science*, 62:450 – 465.

Drury, J., Brown, R., González, R., and Miranda, D. (2015). Emergent social identity and observing social support predict social support provided by survivors in a disaster: Solidarity in the 2010 chile earthquake. *European Journal of Social Psychology*, 46(2):209–223.

Filippidis, L., Galea, E., Gwynne, S., and Lawrence, P. (2006). Representing the influence of signage on evacuation behavior within an evacuation model. *Journal of Fire Protection Engineering*, 16:37–73.

Galea, R. E., Xie, H., and Lawrence, J. P. (2014). Experimental and survey studies on the effectiveness of dynamic signage systems. *Fire Safety Science*, 11:1129–1143.

Garcimartín, A., Zuriguel, I., Pastor, J., Martín-Gómez, C., and Parisi, D. (2014). Experimental evidence of the "faster is slower" effect. *Transportation Research Procedia*, 2:760 – 767. The Conference on Pedestrian and Evacuation Dynamics 2014 (PED 2014), 22-24 October 2014, Delft, The Netherlands.

Gu, Z., Liu, Z., Shiwakoti, N., and Yang, M. (2016). Video-based analysis of school students' emergency evacuation behavior in earthquakes. *International Journal of Disaster Risk Reduction*, 18:1 – 11.

Haghani, M. (2020a). Empirical methods in pedestrian, crowd and evacuation dynamics: Part i. experimental methods and emerging topics. *Safety Science*, 129:104743.

Haghani, M. (2020b). Empirical methods in pedestrian, crowd and evacuation dynamics: Part ii. field methods and controversial topics. *Safety Science*, 129:104760.

Haghani, M., Sarvi, M., Shahhoseini, Z., and Boltes, M. (2016). How simple hypothetical-choice experiments can be utilized to learn humans' navigational escape decisions in emergencies. *PLOS ONE*, 11(11):1–24.

Harada, Y., Mitsudo, H., and Ohyama, J. (2020). The effect of unusualness on the functional field of view in unsafe scenes. *Visual Cognition*, 28:1–13.

Helbing, D., Farkas, I., and Vicsek, T. (2000). Simulating dynamical features of escape panic. *Nature*, 407(28):487–490.

Ji, Q., Xin, C., Tang, S., and Huang, J. (2017). Symmetry associated with symmetry break: revisiting ants and humans escaping from multiple-exit rooms. *Physica A*.

Latané, B. and Darley, J. M. (1968). Group inhibition of bystander intervention in emergencies. *Journal of Personality and Social Psychology*, 10(3):215–221.

Li, X., Guo, F., Kuang, H., Geng, Z., and Fan, Y. (2019). An extended cost potential field cellular automaton model for pedestrian evacuation considering the restriction of visual field. *Physica A: Statistical Mechanics and its Applications*, 515:47 – 56.

Li, Y., Zhang, P., and Zhang, H. (2017). Study on the location of building evacuation indicators based on eye tracking. In *Proceedings of the 3rd ACM SIGSPATIAL Workshop on Emergency Management Using*, EM-GIS'17, New York, NY, USA. Association for Computing Machinery.

Loftus, E., Loftus, G., and Messo, J. (1987). Some facts about "weapon focus.". *Law and Human Behavior*, 11:55.

Lovreglio, R., Fonzone, A., dell'Olio, L., and Ibeas, A. (2014). The role of herding behaviour in exit choice during evacuation. *Procedia - Social and Behavioral Sciences*, 160:390–399.

Ma, Y., Lee, E. W. M., and Shi, M. (2017). Dual effects of guide-based guidance on pedestrian evacuation. *Physics Letters A*, 381(22):1837 – 1844.

Mackworth, N. H. (1965). Visual noise causes tunnel vision. *Psychonomic Science*, 3.

Mas, E., Suppasri, A., Imamura, F., and Koshimura, S. (2012). Agent-based simulation of the 2011 great east

japan earthquake/tsunami evacuation: An integrated model of tsunami inundation and evacuation. *Journal of Natural Disaster Science*, 34(1):41–57.

Miura, T. (1986). Coping with situational demands: A study of eye movements and peripheral vision performance. In Gale, A. G., Freeman, M. H., Haslegrave, C. M., Smith, P., and Taylor, S. P., editors, *Vision in vehicles*, pages 205–216. North holland Press.

Nilsson, D., Frantzich, H., and Saunders, W. (2009). Influencing exit choice in the event of a fire evacuation. *Fire Safety Science*, 9:341–352.

Nilsson, D. and Johansson, A. (2009). Social influence during the initial phase of a fire evacuation—analysis of evacuation experiments in a cinema theatre. *Fire Safety Journal*, 44(1):71 – 79.

Raafat, R. M., Chater, N., and Frith, C. (2009). Herding in humans. *Trends in Cognitive Sciences*, 13(10):420–428.

Recarte, M. and Nunes, L. (2003). Mental workload while driving: Effects on visual search, discrimination, and decision making. *Journal of experimental psychology. Applied*, 9:119–37.

Saloma, C., Perez, G. J., Tapang, G., Lim, M., and Palmes-Saloma, C. (2003). Self-organized queuing and scale-free behavior in real escape panic. *PNAS*, 100(21):11947–11952.

Schmidt, S. and Galea, E., editors (2013). *Behaviour - Security - Cluture (BeSeCu): Human behaviour in emergencies and disasters: A cross-cultural investigation*. Pabst Science Publishers.

Sieben, A., Schumann, J., and Seyfried, A. (2017). Collective phenomena in crowds-where pedestrian dynamics need social psychology. *PLoS ONE*, 12:1–19.

Tsurushima, A. (2019). Modeling herd behavior caused by evacuation decision making using response threshold. In Davidsson, P. and Verhagen, H., editors, *Multi-Agent-Based Simulation XIX. MABS2018. Lecture Notes in Computer Science, vol 11463*, pages 138–152. Springer.

Tsurushima, A. (2020). Validation of evacuation decision model: An attempt to reproduce human evacuation behaviors during the great east japan earthquake. In *Proceedings of the 12th International Conference on Agents and Artificial Intelligence - Volume 1: ICAART,*, pages 17–27. INSTICC, SciTePress.

Wilensky, U. (1999). *NetLogo*. Center for Connected Learning and Computer-Based Modeling, Northwestern University, Evanston, IL.

Xu, Y. and Huang, H.-J. (2012). Simulation of exit choosing in pedestrian evacuation with consideration of the direction visual field. *Physica A: Statistical Mechanics and its Applications*, 391(4):991 – 1000.

Yang, X., Wu, Z., and Li, Y. (2011). Difference between real-life escape panic and mimic exercises in simulated situation with implications to the statistical physics models of emergency evacuation: The 2008 wenchuan earthquake. *Physica A: Statistical Mechanics and its Applications*, 390(12):2375 – 2380.

Yuan, Z., Jia, H., Zhang, L., and Bian, L. (2017). A social force evacuation model considering the effect of emergency signs. *SIMULATION: Transactions of the Society for Modeling and Simulation International*, page 003754971774135.

Yue, H., Guan, H., Shao, C., and Liu, Y. (2010). Simulation of pedestrian evacuation with affected visual field and absence of evacuation signs. In *2010 Sixth International Conference on Natural Computation*, volume 8, pages 4286–4290.

Zhou, M., Dong, H., Liu, J., Yao, X., and Li, Y. (2018). Modeling of crowd dynamics with emergency signs via modified social force model*. pages 235–240.

APPENDIX

Table 3 shows the results of the parameter searches using black-box simulation in descending order of $\bar{O}$. Searches were conducted 20 times with different initial points.

Table 3: Results of black-box optimization.

ε	δ	α	d	ω	Δr	$\hat{N}$	g	$\bar{O}$
0.1	1.2	0.1	10	20	5.0	15	0.4	28.95
0.1	0.7	0.4	10	20	2.0	1	1.5	27.76
0.1	1.1	0.8	8	20	5.0	2	1.4	26.64
0.2	0.6	0.6	9	20	2.5	7	1.4	26.23
0.1	1.0	0.2	10	20	1.5	20	0.2	26.22
0.2	1.9	1.9	10	10	1.5	6	1.3	25.96
0.3	1.8	0.9	6	20	4.5	19	0.3	23.43
1.0	0.5	0.7	10	10	4.5	13	1.6	22.27
0.6	0.6	1.4	7	10	5.0	4	1.9	22.16
0.1	1.2	0.9	7	20	4.0	2	1.1	22.04
0.3	1.9	0.7	6	20	3.0	15	1.1	22.01
0.7	0.3	0.7	10	10	2.5	2	1.4	21.96
0.4	0.7	0.0	6	20	1.5	4	1.0	21.92
0.7	0.5	1.2	3	70	3.5	16	1.0	15.76
1.0	1.7	1.6	3	70	3.0	1	1.4	15.59
0.8	0.6	0.2	3	80	1.0	7	0.4	12.91
0.6	1.6	1.2	3	70	3.5	1	0.5	12.87
0.8	1.8	1.4	3	70	3.0	1	0.1	12.03
0.8	0.2	1.8	4	360	4.0	11	0.4	-5.95
0.4	1.7	0.0	5	330	2.0	10	0.8	-6.88